Title

Enhancing electrochemical intermediate solvation through electrolyte anion selection to increase nonaqueous Li–O2 battery capacity

Journal

Proceedings of the National Academy of Sciences of the United States of America, 112(30)

ISSN

0027-8424

Authors

Burke, Colin M
Pande, Vikram
Khetan, Abhishek
et al.

Publication Date

2015-07-28

DOI

10.1073/pnas.1505728112

Peer reviewed

Enhancing electrochemical intermediate solvation through electrolyte anion selection to increase nonaqueous Li–O_2 battery capacity

Colin M. Burke[a,b], Vikram Pande[c], Abhishek Khetan[d], Venkatasubramanian Viswanathan[c,1], and Bryan D. McCloskey[a,b,1]

[a]Department of Chemical and Biomolecular Engineering, University of California, Berkeley, CA 94720; [b]Environmental Energy Technologies Division, Lawrence Berkeley National Laboratory, Berkeley, CA 94720; [c]Department of Mechanical Engineering, Carnegie Mellon University, Pittsburgh, PA 15213; and [d]Institute for Combustion Technology, Rheinisch-Westfälische Technische Hochschule Aachen, 52056 Aachen, Germany

Edited by Harold Kung, Northwestern University, Evanston, IL, and accepted by the Editorial Board June 22, 2015 (received for review March 26, 2015)

Among the "beyond Li-ion" battery chemistries, nonaqueous Li–O_2 batteries have the highest theoretical specific energy and, as a result, have attracted significant research attention over the past decade. A critical scientific challenge facing nonaqueous Li–O_2 batteries is the electronically insulating nature of the primary discharge product, lithium peroxide, which passivates the battery cathode as it is formed, leading to low ultimate cell capacities. Recently, strategies to enhance solubility to circumvent this issue have been reported, but rely upon electrolyte formulations that further decrease the overall electrochemical stability of the system, thereby deleteriously affecting battery rechargeability. In this study, we report that a significant enhancement (greater than fourfold) in Li–O_2 cell capacity is possible by appropriately selecting the salt anion in the electrolyte solution. Using ^{7}Li NMR and modeling, we confirm that this improvement is a result of enhanced Li^+ stability in solution, which, in turn, induces solubility of the intermediate to Li_2O_2 formation. Using this strategy, the challenging task of identifying an electrolyte solvent that possesses the anticorrelated properties of high intermediate solubility and solvent stability is alleviated, potentially providing a pathway to develop an electrolyte that affords both high capacity and rechargeability. We believe the model and strategy presented here will be generally useful to enhance Coulombic efficiency in many electrochemical systems (e.g., Li–S batteries) where improving intermediate stability in solution could induce desired mechanisms of product formation.

donor number | solubility | lithium nitrate | NMR | Li–air battery

The lithium–oxygen (Li–O_2) battery has garnered significant research interest in the past 10 y due to its high theoretical specific energy compared with current state-of-the-art lithium-ion (Li-ion) batteries (1, 2). Consisting of a lithium anode and an oxygen cathode, the nonaqueous Li–O_2 battery operates via the electrochemical formation and decomposition of lithium peroxide (Li_2O_2). The ideal overall reversible cell reaction is therefore

$$2Li + O_2 \leftrightarrow Li_2O_2\ (2e^-\ \text{process})\ U = 2.96\ V. \quad [1]$$

One challenge preventing the realization of a modest fraction of the Li–O_2 battery's high theoretical specific energy is that the discharge product, Li_2O_2, which is generally insoluble in aprotic organic electrolytes, is an insulator (3–5). As Li_2O_2 is conformally deposited on the cathode's carbon support during discharge, it electronically passivates the cathode, resulting in practical capacities much smaller than theoretically attainable (6). Recently, two reports described the engineering of electrolytes to circumvent this passivation and improve Li–O_2 battery discharge capacity. Aetukuri et al. suggested that adding ppm quantities of water to a 1,2-dimethoxyethane (DME)-based electrolyte increases the solubility of intermediates during Li_2O_2 formation (7). This increased solubility allows a reduced oxygen species shuttling mechanism that promotes deposition of Li_2O_2 aggregated toroid structures. The diffusion of the intermediates away from the electrode surface allows the surface to remain electronically accessible to Li^+ and O_2, promoting more Li_2O_2 growth, thereby leading to an increase in cell capacity. Of note, this increase in cell capacity with water content in the electrolyte is also consistent with reports by Gasteiger and coworkers (8, 9). Aetukuri et al. reason that this increase could be attributed to water's significantly higher Gutmann Acceptor Number (AN) than DME, as the AN is a measure of a solvent's Lewis acidity, and thus quantifies its ability to efficiently solubilize negatively charged species, such as the potential discharge product intermediate, superoxide (O_2^-) (10). In a related analysis, Johnson et al. showed that an electrolyte solvent with a higher Gutmann Donor Number (DN), a measure of Lewis basicity (11), is more likely to induce toroid formation due to increased Li^+ stability in solution, inducing solubility of O_2^- (12). Johnson et al. further confirmed the presence of O_2^- ions in Li^+-bearing high-DN electrolytes using surface-enhanced Raman spectroscopy (12).

Whereas water and certain organic solvents increase cell capacity via this solution mechanism, there is evidence that both decrease electrolyte stability. Water impurities in Li-ion electrolytes are known to enhance parasitic electrochemical side reactions, and Aetukuri et al. and Cho et al. showed that adding ppm quantities of water in Li–O_2 batteries leads to a decrease in electrolyte stability and increase in irreversible reactions with the

Significance

The Li–air battery has attracted significant interest as a potential high-energy alternative to Li-ion batteries. However, the battery discharge product, lithium peroxide, is both electronically insulative and insoluble in nonaqueous electrolytes. It therefore passivates the battery cathode as it is uniformly deposited and disallows the battery to achieve even a modest fraction of its potential electrochemical capacity. Our objective is to circumvent this challenge by enhancing the solubility of electrochemically formed intermediate species. We present a rational basis for electrolyte (i.e., solvent and salt) selection for nonaqueous Li–air batteries and demonstrate a selection criterion for an electrolyte salt that increases the stability of Li^+ in solution, thereby triggering a solution-based process that allows significantly improved battery capacities.

Author contributions: C.M.B., V.V., and B.D.M. designed research; C.M.B., V.P., and A.K. performed research; C.M.B., V.P., and A.K. analyzed data; and C.M.B., V.P., A.K., V.V., and B.D.M. wrote the paper.

The authors declare no conflict of interest.

This article is a PNAS Direct Submission. H.K. is a guest editor invited by the Editorial Board.

[1]To whom correspondence may be addressed. Email: venkvis@cmu.edu or bmcclosk@berkeley.edu.

This article contains supporting information online at www.pnas.org/lookup/suppl/doi:10.1073/pnas.1505728112/-/DCSupplemental.

ENGINEERING

lithium anode (7, 13). Furthermore, using quantitative measures of battery rechargeability, high-DN solvents, such as DMSO and *N*-methyl pyrrolidone, have been observed to be less stable than low-DN solvents, such as acetonitrile and DME (14). Recently, Khetan et al. used a thermodynamic analysis to show that an organic solvent's ability to induce the solution mechanism is anticorrelated with its stability toward nucleophilic attack (15). Thus, Li–O_2 cells would benefit from an appropriately engineered electrolyte that both induces Li_2O_2 intermediate solubility and maintains or exceeds present electrolyte stability.

In this article, we describe the importance of the lithium salt anion in enhancing the solvation of electrochemically formed intermediate species during Li–O_2 battery discharge, thereby enhancing discharge capacity. We present a study on two common Li–O_2 battery salts, lithium bis(trifluoromethane) sulfonimide (LiTFSI) and lithium nitrate ($LiNO_3$), dissolved in DME. These salts were selected because Schmeisser et al. found that $TFSI^-$ and NO_3^- anions provided different DN in ionic liquids with common cations (NO_3^--containing ILs having higher DN than $TFSI^-$-containing ILs). We also specifically selected NO_3^- because of its reported positive influence on Li–O_2 battery rechargeability compared with the more commonly used $TFSI^-$ (16, 17). We found that electrolytes containing a high concentration of NO_3^- exhibited higher donicity, as verified using ^{7}Li NMR, and provided an increase in battery capacity greater than fourfold compared with a battery using exclusively $TFSI^-$ as the electrolyte anion, while not decreasing battery rechargeability, as measured using quantitative oxygen consumption and evolution. To theoretically quantify this enhancement, we propose an Ising model description of the solvation shell of Li^+. This analysis indicates that the origin of this enhanced solution process is due to the formation of ion pairs (Li^+–NO_3^-) in a DME solvent. The theoretical analysis further predicts that ion-pair formation and the associated enhancement in capacity would not be observed when DMSO is used as a solvent, which was subsequently confirmed experimentally. We generalize this analysis to provide a rational basis for selection of electrolyte (solvent + salt) combinations for use in Li–O_2 batteries. We believe these results will have profound implications not only for Li–O_2 batteries, where a practical outcome of the solubility is an enhancement in battery capacity, but also for other electrochemical systems (e.g., lithium–sulfur batteries) in which intermediate solvation may induce desired mechanisms of product formation.

Results and Discussion

To characterize the effects of the electrolyte salt anion on discharge performance, Li–O_2 cells were prepared with electrolytes of varying concentrations of $LiNO_3$ and LiTFSI salts, totaling 1.0 M Li^+, in DME. Cell design and preparation are detailed in *SI Appendix* and follow those described previously (18).

Fig. 1*A* presents representative galvanostatic discharge profiles of these Li–O_2 cells as a function of the $LiNO_3$ salt concentration. Fig. 1*A* (*Inset*) shows the average cell capacity for each $LiNO_3$ salt concentration. Cell capacity increases more than fourfold over the $LiNO_3$ concentration range studied, clearly indicating the substantial effect of the Li^+ counterion on cell capacity.

Scanning electron microscopy (SEM) was performed on discharged cathodes to investigate changes in Li_2O_2 morphology, and hence changes in discharge mechanism, with increasing $LiNO_3$ concentration. Fig. 2 presents SEM images of a pristine cathode (Fig. 2*A*) and images of cathodes from cells of identical electrolyte compositions as those studied in Fig. 1, but discharged at 45 μA/cm^2 (Fig. 2 *B*–*F*). When comparing Fig. 2 *A*–*C*, the pristine, 0 M $LiNO_3$, and 0.01 M $LiNO_3$ cathodes appear indistinguishable. This implies a conformal coating of discharge product on the 0 M $LiNO_3$ and 0.01 M $LiNO_3$ cathodes, and is consistent with previous reports for 1 M LiTFSI in DME (7, 19).

A conformal coating of discharge product is indicative of a predominant thin-film Li_2O_2 surface deposition mechanism. Originally outlined by Laoire et al., this mechanism is described by the following elementary steps (20, 21):

$$Li^+ + e^- + O_2^* \leftrightarrow LiO_2^*, \qquad [2]$$

$$Li^+ + e^- + LiO_2^* \leftrightarrow Li_2O_2^* \text{ and/or } 2LiO_2^* \leftrightarrow Li_2O_2^* + O_2, \qquad [3a,b]$$

where "*" denotes a species adsorbed to the cathode/Li_2O_2 surface. Importantly, in the LiTFSI/DME electrolyte, LiO_2* is insoluble and therefore remains adsorbed to the electrode surface, where a second charge transfer step (reaction **3a**) or a disproportionation reaction (reaction **3b**) results in the conformal Li_2O_2 coating observed in Fig. 2 *B* and *C* (2, 19–23).

As the $LiNO_3$:LiTFSI ratio increases, the discharge morphology changes perceptibly. As seen in Fig. 2*D*, when using 0.1 M $LiNO_3$, nodular morphologies appear on the cathode surface. Increasing the $LiNO_3$ concentration to 0.5 M and 0.7 M finds these structures replaced with increasingly larger toroid structures, as seen in Fig. 2 *E* and *F*, respectively.

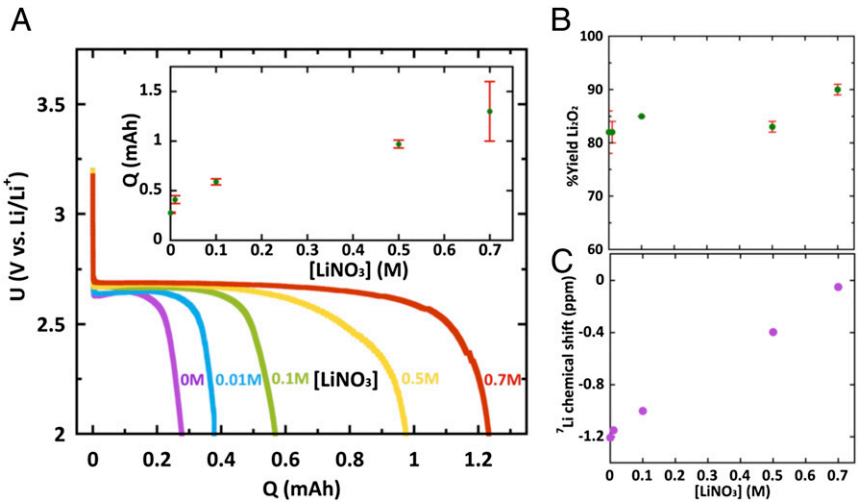

Fig. 1. (*A*) Representative galvanostatic discharge profiles of Li–O_2 cells (450 μA/cm^2 under a 1.5-atm O_2 atmosphere to a 2-V cutoff). (*Inset*) Capacity dependence on $LiNO_3$ concentration. (*B*) Li_2O_2 discharge yield as a function of $LiNO_3$ electrolyte concentration. (*C*) ^{7}Li chemical shift of electrolyte solutions, versus a 3 M LiCl in D_2O standard, as a function of electrolyte $LiNO_3$ concentration. A less negative chemical shift represents a shift down-field. A 1.0 M Li^+ concentration was used for all electrolytes (DME used as the solvent), and the LiTFSI:$LiNO_3$ ratio was varied. The $LiNO_3$ concentration for each cell is provided in the figure. As an example, the cell labeled "0.1 M $LiNO_3$" contained 0.1 M $LiNO_3$ and 0.9 M LiTFSI. Error bars are 1 SD of multiple experiments.

As described previously, the toroid morphology observed in Fig. 2 *D–F* is indicative of a solution mechanism of Li_2O_2 growth proceeding through solubility of the LiO_2 intermediate (7, 12, 24). The dissolution of LiO_2* into lithium cations and the redox active superoxide anion, O_2^-, follows the equilibrium reaction (7):

$$LiO_2^* \leftrightarrow Li^+(sol) + O_2^-(sol). \quad [4]$$

Solvated O_2^- can then diffuse in solution to a growing Li_2O_2 toroid, where it can combine with Li^+ to form adsorbed LiO_2* on the toroid surface. LiO_2* can subsequently undergo disproportionation according to Eq. **3b**, leading to the formation of Li_2O_2 on the toroid surface (7). The observed toroid formation on discharged cathodes from cells using high $LiNO_3$:LiTFSI ratios supports the enhancement of this solution mechanism with increasing $LiNO_3$ concentration.

In further support of the solution mechanism, increasingly larger toroid structures were observed with decreasing current density in cells using 0.5 M $LiNO_3$ (0.5 M LiTFSI) (*SI Appendix*, Fig. S1). This observation is consistent with previous reports where Li_2O_2 toroid formation was observed at low currents in electrolytes that promoted the solution Li_2O_2 formation mechanism (7, 12, 24).

Of note, we find that Li_2O_2 yield, as measured using an established peroxide titration technique (18), is generally unaffected by the electrolyte compositions studied here (Fig. 1*B*), although a slightly higher Li_2O_2 yield may be observed at high $LiNO_3$ concentrations. Differential electrochemical mass spectrometry was also used, as described previously (18), to quantify the reversibility of the electrochemical reactions (*SI Appendix*, Fig. S2). The ratio (OER:ORR) of the amount of oxygen evolved during charge (OER) to the amount of oxygen consumed during discharge (ORR), an important metric of reversibility, is statistically

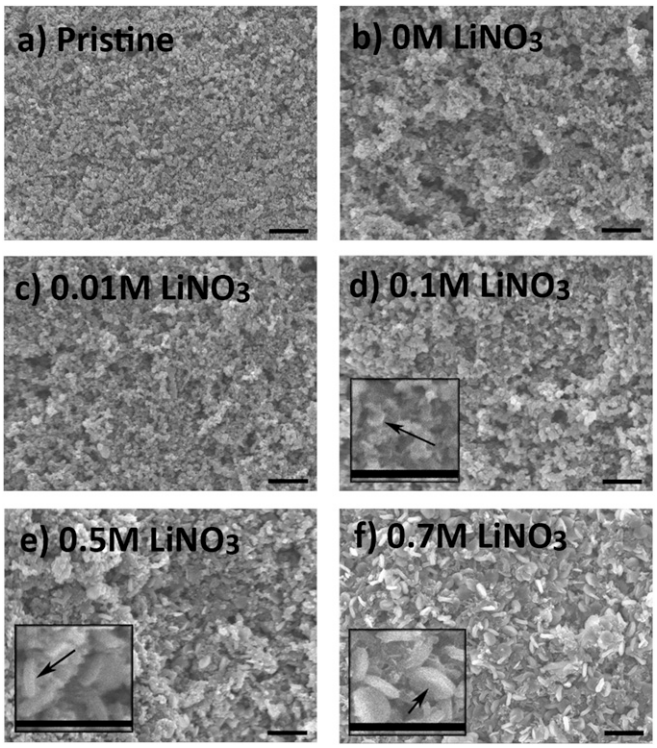

Fig. 2. (*A*) SEM image of pristine XC72 carbon cathode before discharge. (*B–F*) Discharged cathodes from cells using 1 M total Li^+ concentration, with 0 M $LiNO_3$ (1 M LiTFSI), 0.01 M $LiNO_3$, 0.1 M $LiNO_3$, 0.5 M $LiNO_3$, and 0.7 M $LiNO_3$, respectively. Cells were discharged at 45 μA/cm^2 to 0.9 mAh/cm^2 or a 2-V cutoff voltage. All cells had at least 0.5 mAh/cm^2 capacity. (Scale bars, 1 μm.)

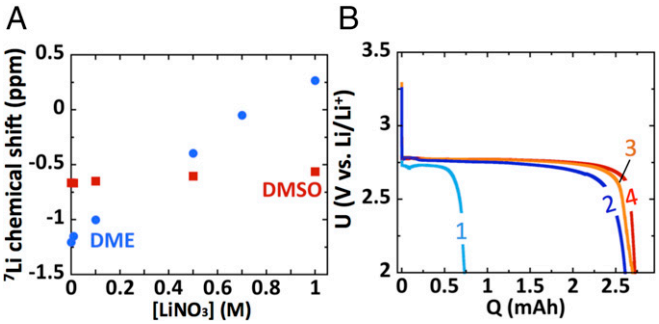

Fig. 3. (*A*) ^{7}Li chemical shift of DMSO and DME-based electrolytes, versus a 3 M LiCl in D_2O reference, as a function of electrolyte $LiNO_3$ concentration. A less negative chemical shift represents a shift down-field. A 1.0 M Li^+ concentration was used for all cell electrolytes, and the LiTFSI:$LiNO_3$ ratio was varied. (*B*) Discharge profiles (45 μA/cm^2, 2-V cutoff) for cells employing DMSO and DME-based electrolytes. Labels correspond to discharges of cells using the following electrolytes: **1**. 1 M LiTFSI in DME, **2**. 0.5 M $LiNO_3$:0.5 M LiTFSI in DME, **3**. 1 M LiTFSI in DMSO, and **4**. 0.5 M $LiNO_3$:0.5 M LiTFSI in DMSO.

equal for a cell using 1 M LiTFSI and a cell using 0.5 M $LiNO_3$:0.5 M LiTFSI (OER:ORR ~0.82). Furthermore, only $^{18}O_2$ is evolved on charge after a discharge under $^{18}O_2$ of a cell using 0.5 M $LiN^{16}O_3$:0.5 M LiTFSI, confirming that NO_3^- does not participate in the cathode reaction other than to induce solubility of the intermediates. This result agrees with a similar experiment using pure LiTFSI-based electrolytes (19), implying that electroactive O_2 remains associated during both Li_2O_2 formation and oxidation.

With a change in anion clearly inducing a solution Li_2O_2 growth mechanism, it can be reasoned that the NO_3^- anion is affecting LiO_2 solubility via enhanced Li^+ solvation. The electrolyte anion can affect the electrolyte's overall donicity [quantified by the Gutmann DN, a measure of Lewis basicity (11)], in turn affecting the electrolyte's ability to solubilize LiO_2* through enhanced solvation of Li^+. We used ^{7}Li NMR to probe the electron donicity felt by Li^+ ions in our $LiNO_3$:LiTFSI in DME electrolytes as a proxy measurement of the relative effect of the anion on electrolyte DN.

Using NMR as a proxy for DN is a well-known technique, with Erlich and Popov first proposing ^{23}Na NMR as an effective measurement for a solvent's DN (25). Erlich and Popov reasoned that a down-field ^{23}Na shift resulted from stronger interaction between the solvation shell molecules and the cation, thereby decreasing the cation's shielding. The environment of Li^+ in $LiNO_3$:LiTFSI in DME electrolytes cannot be determined via ^{23}Na NMR, as adding $NaClO_4$ to the electrolytes causes a white precipitate to crash out of solution [likely $NaNO_3$, as dissolving $NaClO_4$ in an anhydrous solvent containing $LiNO_3$ has been proposed as a method for making anhydrous $LiClO_4$ (26)]. However, we reason that ^{7}Li NMR, in place of ^{23}Na NMR, can serve as a reasonable proxy of the relative donicity of Li^+ electrolytes in a single solvent.

Fig. 1*C* shows the ^{7}Li chemical shift, referenced to an external standard of LiCl in D_2O, of each $LiNO_3$:LiTFSI in DME electrolyte. As $LiNO_3$ concentration increases, the ^{7}Li peak shifts down-field, or becomes less shielded. Cahen et al. showed that the ^{7}Li chemical shift of a lithium salt may display a concentration dependence, contingent, to a first approximation, on the DN of the solvent and the DN of the anion (27). The DN of an electrolyte containing a low-DN solvent and a high-DN anion, like Br^- (DN = 33.7 kcal/mol) in acetonitrile (DN = 14.1 kcal/mol), exhibits an anion concentration dependence [DN values from Linert et al. (28)]. Conversely, electrolytes comprising a high-DN solvent with a relatively low DN anion, like ClO_4^- (DN = 8.44 kcal/mol) in dimethyl sulfoxide (DN = 29.8 kcal/mol), do

ENGINEERING

not exhibit a DN dependence on anion concentration. These trends agree with Linert et al., who found via solvatochromic dyes that the effective DN of an electrolyte depended on an interplay between the DN of the solvent, DN of the anion, and AN of the solvent (28). For example, if the solvent's DN was larger than the anion's DN, then the electrolyte comprising the two had a DN similar to its solvent's DN.

If $LiNO_3$ indeed has a higher DN than DME, then increasing the concentration of $LiNO_3$ will increase the number of NO_3^- interacting with any particular Li^+, which in turn will lead to an increase in the electrolyte's DN. Thus, we reason that the presence of a concentration dependence on ^7Li chemical shift, as seen in Fig. 1*C*, indicates NO_3^- serving an active role in the electrolyte's donicity, and the increasingly down-field shift of ^7Li with increasing $LiNO_3$ concentration represents increasing donicity.

In contrast, Fig. 3 shows that indeed $LiNO_3$:LiTFSI salts in the high-DN solvent dimethyl sulfoxide do not exhibit a substantial change in ^7Li shift with increasing $LiNO_3$ concentration, and, as therefore expected, no statistically significant capacity increase is observed in DMSO-based electrolytes as the $LiNO_3$:TFSI ratio increases. To confirm the general correlation between enhanced Li^+ solvation and Li–O_2 battery capacity, another high-DN anion, Br^-, was studied. As expected, similar trends in ^7Li NMR chemical shifts and Li–O_2 battery capacity are observed between 0.5M LiBr:0.5M LiTFSI and 0.5 M $LiNO_3$:0.5 M LiTFSI in DME and DMSO-based electrolytes (*SI Appendix*, Fig. S10).

We note, however, that extreme care must be taken when using NMR techniques to compare and quantify solvent DNs, particularly between dislike solvent classes, such as protic and aprotic solvents, as was discussed by Gal and Laurence (29). For the current study, our interest is only in the relative changes of the Li^+ chemical environment as a function of anion composition in a single aprotic solvent (both for DME and DMSO), such that ^7Li NMR provides useful qualitative, if not quantitative, values for comparison.

To provide a quantitative basis for the role played by the electrolyte anion, we present a revised thermodynamic model for the solution electrochemical process. The solution-mediated electrochemical growth of Li_2O_2 is triggered by the dissolution reaction given in Eq. 4. The free-energy change involved in this dissolution reaction is given by

$$\Delta G_{sol} = G_{Li^+_{sol}} + G_{O^-_{2,sol}} - G_{LiO^*_2}\,, \qquad [5]$$

where $G_{Li^+_{sol}}$ is the free energy of the Li^+ ions in the electrolyte, $G_{O^-_{2,sol}}$ is the free energy of O_2^- ions in the electrolyte, and $G_{LiO^*_2}$ is the free energy of the adsorbed LiO_2 on the Li_2O_2 surface during discharge.

To understand the role of the salt anion on the equilibrium of the dissolution reaction, we need to explore the stabilization of the solvated intermediates in the presence of the anion. The presence of the anion can influence the free energy of Li^+ ions. To a first approximation, the free energy of the Li^+ ions and thus the free energy of LiO_2 dissolution is largely dependent on the species that are present in the Li^+ first solvation shell (30, 31). To be consistent with the experimental data presented in Figs. 1–3, we explicitly model an electrolyte that contains a mixture of $LiNO_3$ and LiTFSI such that the total Li^+ concentration is maintained at 1 M. The concentration of O_2^- ions in the solution is expected to be much lower than the Li^+ and salt anion concentrations (7). Thus, we do not expect O_2^- ions to play a significant role in the solvation of Li^+. Hence, to a first approximation, the solvation shell of Li^+ will comprise only solvent molecules and salt anions (NO_3^- and $TFSI^-$). The exact composition of the solvation shell will depend on the energetics of the interactions of the Li^+ ion with the solvent and the anions. To determine the composition of the first solvation shell and in turn the free energy of stabilization, we develop a modified Ising model for the site occupancy in the solvation shell of Li^+ (32). The Ising model formalism, originally developed to describe magnetism, provides a systematic basis for treating the energetics of interaction between Li^+ and the solvent and salt anions (33).

In this model, we develop a site occupancy variable to describe each of the solvation shell sites of Li^+. The Hamiltonian that governs the solvation shell of Li^+ is given by

$$\begin{aligned} H = {} & h_1 \sum_{i=1}^{N} n_i + h_2 \sum_{i=1}^{N} m_i + h_3 \sum_{i=1}^{N} l_i + J_{11} \sum_{\langle i,j\rangle} n_i n_j + J_{22} \sum_{\langle i,j\rangle} m_i m_j \\ & + J_{33} \sum_{\langle i,j\rangle} l_i l_j + J_{12} \sum_{\langle i,j\rangle} n_i m_j + J_{21} \sum_{\langle i,j\rangle} m_i n_j + J_{13} \sum_{\langle i,j\rangle} n_i l_j \\ & + J_{31} \sum_{\langle i,j\rangle} l_i n_j + J_{23} \sum_{\langle i,j\rangle} m_i l_j + J_{32} \sum_{\langle i,j\rangle} l_i m_j, \end{aligned} \qquad [6]$$

where i = 1 to N represent sites in the solvation shell of a Li^+ ion and $\langle i,j\rangle$ represents the nearest-neighbor pair in the solvation shell. The occupation variables "n," "m," and "l" represent the occupancy of a site by the solvent, the NO_3^- anions, and the $TFSI^-$ anions, respectively. For any site "i" occupied by the solvent, $n_i = 1$, $m_i = 0$, and $l_i = 0$ and similarly for other cases. Thus, at any given site, $n_i + m_i + l_i = 1$, i.e., each site is occupied by either solvent or a salt anion. In our model, h_1 represents the interaction energy between a Li^+ ion and a solvent, h_2 represents the interaction energy between a NO_3^- anion and Li^+, and h_3 represents the interaction energy between a $TFSI^-$ anion and Li^+. The coupling constant J_{11} represents the interaction between neighboring solvent molecules in the Li^+ solvation shell. Likewise, J_{22} and J_{33} represent the interactions between neighboring NO_3^- and neighboring $TFSI^-$ anions, respectively. The symmetry assumption is invoked, which yields $J_{12} = J_{21}$, $J_{13} = J_{31}$, $J_{23} = J_{32}$. The cross-coupling terms J_{12}, J_{13}, and J_{23} represent interactions between neighboring NO_3^- and solvent molecules, neighboring $TFSI^-$ and solvent molecules, and neighboring $TFSI^-$ and NO_3^- anions, respectively.

The exact model is not easily analytically tractable; however, we can invoke the mean-field approximation, described in *SI Appendix*. The mean-field approximation is valid under the assumption that the Li^+ ions are uniformly distributed in solution and each site in the solvation shell experiences an averaged effect of other species present in the electrolyte. The coordination number z of the solvation shell is expected to be independent of species (anions or solvent) occupying the solvation shell. The mean-field approximation replaces the nearest-neighbor interaction ($n_i n_j$) by the average interaction ($n_i\langle n\rangle$), where assuming spatial invariance, the average occupation of species in the shell can be defined as $\langle n\rangle = 1/N \sum_{i=1}^{N} \langle n_i\rangle$.

The interaction term h_1 is dependent on the donating tendency of the solvent molecule to the Li^+ ions in solution. The free energy of Li^+ ions can be expressed in terms of the half-wave potential of Li/Li^+ couple and it has been shown that the half-wave potential of Li/Li^+ couple is a function of the DN of the solvent (34). Hence the Li^+–solvent interaction energetics (h_1) can be expressed as a function of the DN of the solvent. Similarly, we assume that the terms h_2 and h_3 can be expressed as a function of the DN. There is an additional contribution to h_2 and h_3 that depends on the concentration of the NO_3^- and $TFSI^-$ anions. This arises due to a change in the reference chemical potential of the NO_3^- and $TFSI^-$ anions to account for the configurational entropy associated with that concentration. The coupling constant J_{11} is a weak attractive van der Waals interaction between solvent molecules, and is estimated to be an order of magnitude less than the donor interactions h_1, h_2, and h_3. The constants J_{22}, J_{33}, and J_{23} are representative of the repulsive interaction between neighboring anions in the Li^+ solvation shell and are of the same order of magnitude as h_1, h_2. The coupling constants J_{12}, J_{13} for the

interaction between a solvent molecule and the respective anion can be described by the electron accepting tendency of the solvent and can therefore be determined by the solvent's AN. As we are accounting for the coupling constants in terms of the overall donating and accepting tendencies of the solvent, the overall coordination number is already included in the model, i.e., z = 2.

Solving *SI Appendix*, Eqs. **S4 *a–c***, we derive analytical expressions for the average occupation numbers of the solvent molecules and the anions in the first solvation shell of the Li^+ ion as functions of the DN of the solvent, DN of the anion, and anion concentration. From the occupation numbers, we can determine the overall free energy of Li^+ ions in solution using the mean-field relation:

$$G_{Li^+} = \langle n \rangle h_1(DN_{sol}) + \langle m \rangle h_2\left(DN_{NO_3^-}, c_{NO_3^-}\right) + \langle l \rangle h_3(DN_{TSFI^-}, c_{TFSI^-}). \quad [7]$$

The developed model requires the DN of NO_3^- and $TFSI^-$ anions to determine the occupation numbers. We use the values determined by Schmeisser et al. via ^{23}Na NMR for ionic liquids with common cations, as discussed earlier (35). Although the quantitative nature of these measurements is still under debate (29), we believe the trends can be well captured from these values. Schmeisser et al. find that $TFSI^-$ has a very low DN of 11.2 kcal/mol whereas NO_3^- has a DN of 22.2 kcal/mol (35). Using these values, we can determine the occupation shell of Li^+ as a function of the NO_3^- anion concentration. As is shown in Fig. 4*A*, the solvation shell is completely dominated by DME and NO_3^- anion. As the NO_3^- anion has a higher DN than DME (DN = 20 kcal/mol), we observe a strong concentration dependence on the NO_3^- anion. This suggests that increasing NO_3^- anion concentration will lead to a displacement of low-DN solvents like DME in the Li^+ solvation shell. As we increase the concentration of NO_3^- in DME, a higher number of NO_3^- ions occupy the Li^+ solvation shell until the electrostatic repulsion of NO_3^- ions becomes dominant, leading to a saturation in the number of anions that occupy the first solvation shell.

The corresponding change in the free energy of Li^+ as a function of NO_3^- concentration in DME is shown in Fig. 4*B*. The free energy of Li^+ as evaluated from the model is well-correlated with the experimentally measured NMR ^7Li chemical shift, as shown in *SI Appendix*, Fig. S8. This proves that the thermodynamic analysis developed in this work accurately captures the effect of the change in anion concentration in the Li^+ solvation shell. Due to a higher DN of the NO_3^- anion, there is an overall increase in Li^+ solvation energy; this is accompanied by an enhancement of the rate of the solution process given by $r_S \sim \exp((-\Delta G_{sol})/kT)$. This shows that

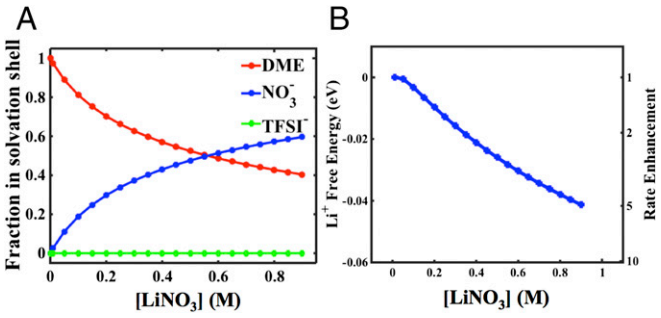

Fig. 4. (*A*) Occupation of the solvent (red line), $TFSI^-$ (green line), and NO_3^- (blue line) in the Li^+ solvation shell and (*B*) the Li^+ solvation energy (eV) as a function of the concentration of the NO_3^- anion. The rate enhancement of the solution process, $r_S \sim \exp((-\Delta G_{sol})/kT)$, is marked on the right *y* axis of *B*. The Li^+ free energy is normalized relative to that of the case with 1 M LiTFSI. There is a rate enhancement, r_S, by a factor of ~4 as the concentration of NO_3^- is increased from 0.1 to 0.5 M.

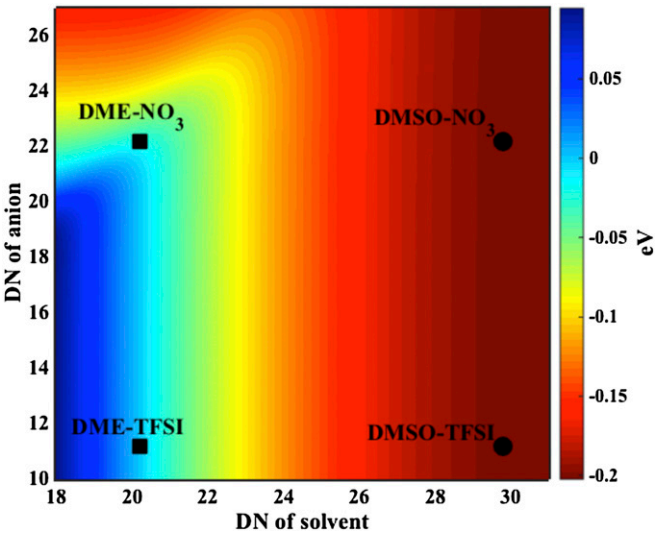

Fig. 5. Contour plot showing the free energy of Li^+ for electrolytes with varying DN of the solvent and salt anion, in kcal/mol. The free energy is normalized relative to that of DME and 1 M LiTFSI. The electrolyte is considered to be a 50:50 mixture of LiTFSI and a salt consisting of Li^+ and the labeled salt anion in the labeled solvent. The blue region corresponds to those electrolytes incapable of triggering the solution process whereas the red region corresponds to those that can trigger the solution process.

at 0.5 M $LiNO_3$:LiTFSI, we would expect an approximately fourfold enhancement in the rate of the solution process. The rate enhancement, $r_S \sim \exp((-\Delta G_{sol})/kT)$, as calculated from the model, shows a positive correlation with the observed capacity enhancement as shown in *SI Appendix*, Fig. S9.

The model developed can be generalized to map out the entire electrolyte design space. A contour map of the Li^+ stabilization as a function of varying DN of solvent and anion is shown in Fig. 5 and the corresponding contour map of the occupation of the solvent in the solvation shell in shown in *SI Appendix*, Fig. S5. This generalization analysis assumes a constant AN chosen to be the average of DME and DMSO and a 50:50 salt blend of LiTFSI and a varying electrolyte anion. The contour map shows that there is an enhancement when using low-DN solvent, such as DME, and high-DN salt anion, such as NO_3^- ions. However, an interesting prediction of this generalized analysis is that there is no benefit in using high-DN salt anions in a high-DN solvent such as DMSO (a more detailed analysis of the DMSO case is reported in *SI Appendix*). This suggests that there is no ion-pair formation in a DMSO solvent and hence, almost no associated change in discharge capacity. This is in excellent agreement with the experiments presented in Fig. 3. To emphasize this agreement, our model predicts that in DMSO, the NO_3^- anion does not enter the Li^+ solvation shell, and hence there is no change in the Li^+ solvation free energy (*SI Appendix*, Figs. S3 and S4).

The contour map suggests that using a higher DN anion than NO_3^- can lead to even greater enhancement of Li^+ solvation, and therefore a study on bromide's (Br^-) effect on Li^+ solvation and Li–O_2 capacity was performed (28). Our model predicts that for an electrolyte consisting of DME as a solvent and LiTFSI and LiBr as the salt blend, there is a greater stabilization of Li^+ compared with the LiTFSI and $LiNO_3$ salt blend of similar concentration, as shown in *SI Appendix*, Fig. S11. The results from the model are consistent with ^7Li NMR chemical shifts (*SI Appendix*, Fig. S10*A* presents the LiBr ^7Li NMR results). We also find a capacity enhancement with the 0.5 M LiBr:0.5 M LiTFSI electrolyte over the 1 M LiTFSI electrolyte (*SI Appendix*, Fig. S10*B*). Of note, the capacity enhancement obtained in our LiBr and $LiNO_3$ studies are statistically similar, although using Li^+

ENGINEERING

solvation arguments alone, the LiBr-containing cells would be expected to have higher capacities at similar electrolyte concentrations. However, in addition to the free energy of dissolution, ΔG_{sol}, other factors, such as O_2 solubility, and the diffusion coefficients of O_2^- and Li^+, govern the overall rate for the solution process and, thereby, the overall capacity enhancement due to the solution process. These other factors likely contribute to suppress the capacity gains expected solely from enhanced solvation when employing the LiBr electrolyte compared to the $LiNO_3$ electrolyte.

The contour map presented in Fig. 5 provides a rational basis for selection of the total electrolyte, i.e., solvent and anion. An important conclusion of the contour map is that there is minimal capacity enhancement by changing the electrolyte anion in high-DN solvents. We have demonstrated this conclusion using two examples of high-DN anions (Br^-, NO_3^-) showing almost no enhancement in solvation in a high-DN solvent such as DMSO as shown in *SI Appendix*, Figs. S3 and S12. However, there is tremendous scope in tuning the electrolyte anion in low-DN solvents to obtain high discharge capacities. Given that it should be simpler to identify anions stable to the Li–O_2 cathode electrochemistry than high-DN solvents (36, 37), anion selection in combination with low-DN solvents potentially provides a route to avoid the unfavorable capacity/stability trade-off observed in high-DN solvents, such as DMSO (14, 15, 38, 39).

Conclusions

In conclusion, we have demonstrated Li^+ counterion influence on promoting the solubility of electrochemical intermediates during a Li–O_2 battery discharge without further compromising electrolyte stability. Specifically, Li–O_2 batteries using electrolytes of $LiNO_3$ and LiTFSI in DME displayed increased capacity and increased toroid formation with increasing $LiNO_3$ concentration. We ascribe intermediate solubility to enhanced stability of Li^+ in solution by anions with higher effective donor numbers than that of the solvent, thereby also inducing increased stability of the electrochemically formed anion, O_2^-, in solution. This strategy can potentially be combined with current efforts to identify novel, stable electrolytes, including those in which organic molecules are entirely removed from the electrolyte [a fascinating idea being explored by researchers at Liox Power, Inc. (40)], to develop a practical electrolyte that could enable high-energy, long-life Li–air batteries. Further, we have developed a generalized model that predicts Li^+ solvation shell occupation and the resulting stability of Li^+ in electrolytic solutions. We envision this strategy for intermediate stabilization to be generally applicable to numerous nonaqueous systems in which stabilization of desired intermediates may lead to improved electrochemical efficiency. For example, in Li–S batteries, polysulfide intermediate speciation could potentially be controlled by simply tuning the Li^+ salt anion, perhaps providing a route for increased sulfur utilization.

ACKNOWLEDGMENTS. The authors thank Alan Luntz, Dan Addison, Jeffrey Reimer, Hilda Buss, Jessica Nichols, and Christopher Dekmezian for helpful discussions and guidance on materials characterization. The work at University of California, Berkeley/Lawrence Berkeley National Laboratory (LBNL) was supported in part by previous work performed through the Laboratory Directed Research and Development Program of LBNL under US Department of Energy Contract DE-AC02-05CH11231. Support for C.M.B. was provided through the US DOE Vehicle Technologies Office under award DE-0006869. A.K. thankfully acknowledges the funding for his doctoral studies from the Deutsche Forschungsgemeinschaft.

1. Christensen J, et al. (2012) A critical review of Li/air batteries. *J Electrochem Soc* 159(2): R1–R30.
2. Luntz AC, McCloskey BD (2014) Nonaqueous Li-air batteries: A status report. *Chem Rev* 114(23):11721–11750.
3. Viswanathan V, et al. (2011) Electrical conductivity in Li_2O_2 and its role in determining capacity limitations in non-aqueous Li-O_2 batteries. *J Chem Phys* 135(21):214704.
4. Meini S, Piana M, Beyer H, Schwämmlein J, Gasteiger HA (2012) Effect of carbon surface area on first discharge capacity of Li-O_2 cathodes and cycle-life behavior in ether-based electrolytes. *J Electrochem Soc* 159(12):A2135–A2142.
5. Gerbig O, Merkle R, Maier J (2013) Electron and ion transport in Li_2O_2. *Adv Mater* 25(22):3129–3133.
6. Højberg J, et al. (2015) An electrochemical impedance spectroscopy investigation of the overpotentials in Li-O_2 batteries. *ACS Appl Mater Interfaces* 7(7):4039–4047.
7. Aetukuri NB, et al. (2015) Solvating additives drive solution-mediated electrochemistry and enhance toroid growth in non-aqueous Li-O_2 batteries. *Nat Chem* 7(1):50–56.
8. Meini S, Piana M, Tsiouvaras N, Garsuch A, Gasteiger HA (2012) The effect of water on the discharge capacity of a non-catalyzed carbon cathode for Li-O_2 batteries. *Electrochem Solid-State Lett* 15(4):A45–A48.
9. Schwenke KU, Metzger M, Restle T, Piana M, Gasteiger HA (2015) The influence of water and protons on Li_2O_2 crystal growth in aprotic Li-O_2 cells. *J Electrochem Soc* 162(4):A573–A584.
10. Mayer U, Gutmann V, Gerger W (1975) The acceptor number—A quantitative empirical parameter for the electrophilic properties of solvents. *Monatsh Chem* 106(6):1235–1257.
11. Gutmann V, Wychera E (1966) Coordination reactions in non aqueous solutions - The role of the donor strength. *Inorg Nucl Chem Lett* 2(9):257–260.
12. Johnson L, et al. (2014) The role of LiO_2 solubility in O_2 reduction in aprotic solvents and its consequences for Li-O_2 batteries. *Nat Chem* 6(12):1091–1099.
13. Cho MH, et al. (2014) The effects of moisture contamination in the Li-O_2 battery. *J Power Sources* 268:565–574.
14. McCloskey BD, et al. (2012) Limitations in rechargeability of Li-O_2 batteries and possible origins. *J Phys Chem Lett* 3(20):3043–3047.
15. Khetan A, Luntz A, Viswanathan V (2015) Trade-offs in capacity and rechargeability in nonaqueous Li–O_2 batteries: solution-driven growth versus nucleophilic stability. *J Phys Chem Lett* 6(7):1254–1259.
16. Walker W, et al. (2013) A rechargeable Li-O_2 battery using a lithium nitrate/N,N-dimethylacetamide electrolyte. *J Am Chem Soc* 135(6):2076–2079.
17. Uddin J, et al. (2013) Lithium nitrate as regenerable SEI stabilizing agent for rechargeable Li/O_2 batteries. *J Phys Chem Lett* 4(21):3760–3765.
18. McCloskey BD, et al. (2013) Combining accurate O_2 and Li_2O_2 assays to separate discharge and charge stability limitations in nonaqueous Li-O_2 batteries. *J Phys Chem Lett* 4:2989–2993.
19. McCloskey BD, Scheffler R, Speidel A, Girishkumar G, Luntz AC (2012) On the mechanism of nonaqueous Li–O_2 electrochemistry on C and its kinetic overpotentials: Some implications for Li–air batteries. *J Phys Chem C* 116(45):23897–23905.
20. Laoire CO, Mukerjee S, Abraham KM, Plichta EJ, Hendrickson MA (2010) Influence of nonaqueous solvents on the electrochemistry of oxygen in the rechargeable lithium-air battery. *J Phys Chem C* 114(19):9178–9186.
21. Laoire CO, Mukerjee S, Abraham KM, Plichta EJ, Hendrickson MA (2009) Elucidating the mechanism of oxygen reduction for lithium-air battery applications. *J Phys Chem C* 113(46):20127–20134.
22. Peng Z, et al. (2011) Oxygen reactions in a non-aqueous Li^+ electrolyte. *Angew Chem Int Ed Engl* 50(28):6351–6355.
23. Lu YC, et al. (2013) Lithium-oxygen batteries: Bridging mechanistic understanding and battery performance. *Energy Environ Sci* 6(3):750–768.
24. Adams BD, et al. (2013) Current density dependence of peroxide formation in the Li-O_2 battery and its effect on charge. *Energy Environ Sci* 6(6):1772–1778.
25. Erlich RH, Popov AI (1971) Spectroscopic studies of ionic solvation. X. Study of the solvation of sodium ions in nonaqueous solvents by sodium-23 nuclear magnetic resonance. *J Am Chem Soc* 93(22):5620–5623.
26. Cretzmeyer JW (1963) Process for producing anhydrous lithium perchlorate, US Patent US3075827.
27. Cahen YM, Handy PR, Roach ET, Popov AI (1975) Spectroscopic studies of ionic solvation. XVI. Lithium-7 and chlorine-35 nuclear magnetic resonance studies in various solvents. *J Phys Chem* 79(1):80–85.
28. Linert W, Jameson RF, Taha A (1993) Donor numbers of anions in solution: The use of solvatochromic Lewis acid-base indicators. *J Chem Soc, Dalton Trans* (21):3181–3186.
29. Gal J-F, Laurence C (2013) Comment on the article "Gutmann donor and acceptor numbers for ionic liquids" by M. Schmeisser, P. Illner, R. Puchta, A. Zahl, and R. van Eldik (Chem Eur J 2012, 18, 10969–10982). *Chemistry* 19(49):16832–16834.
30. Marcus Y (1991) Thermodynamics of solvation of ions. Part 5.-Gibbs free energy of hydration at 298.15 K. *J Chem Soc, Faraday Trans* 87(18):2995–2999.
31. Bryantsev VS, Diallo MS, Goddard WA, 3rd (2008) Calculation of solvation free energies of charged solutes using mixed cluster/continuum models. *J Phys Chem B* 112(32):9709–9719.
32. Sethna J (2006) *Statistical Mechanics: Entropy, Order Parameters, and Complexity* (Oxford Univ Press, New York).
33. Ising E (1925) Beitrag zur theorie des ferromagnetismus. *Z Phys* 31(1):253–258.
34. Gritzner G (1986) Solvent effects on half-wave potentials. *J Phys Chem* 90(21):5478–5485.
35. Schmeisser M, Illner P, Puchta R, Zahl A, van Eldik R (2012) Gutmann donor and acceptor numbers for ionic liquids. *Chemistry* 18(35):10969–10982.
36. Nasybulin E, et al. (2013) Effects of electrolyte salts on the performance of Li-O_2 batteries. *J Phys Chem C* 117(6):2635–2645.
37. Gunasekara I, Mukerjee S, Plichta EJ, Hendrickson MA, Abraham KM (2015) A study of the influence of lithium salt anions on oxygen reduction reactions in Li-air batteries. *J Electrochem Soc* 162(6):A1055–A1066.
38. Kwabi DG, et al. (2014) Chemical instability of dimethyl sulfoxide in lithium–air batteries. *J Phys Chem Lett* 5:2850–2856.
39. Sharon D, et al. (2013) Oxidation of dimethyl sulfoxide solutions by electrochemical reduction of oxygen. *J Phys Chem Lett* 4(18):3115–3119.
40. Uddin J, Addison DD, Giordani V, Chase GV, Walker W (2014) Alkali metal/oxygen batteries employing molten nitrate electrolytes, Patent WO 2014153551.